Article

Lumenal Protein within Secretory Granules Affects Fusion Pore Expansion

Annita Ngatchou Weiss,[1,*] Arun Anantharam,[2] Mary A. Bittner,[1] Daniel Axelrod,[1,3] and Ronald W. Holz[1,*]
[1]Department of Pharmacology, University of Michigan Medical School, Ann Arbor Michigan; [2]Department of Biological Sciences, Wayne State University, Detroit, Michigan; and [3]Department of Physics and LSA Biophysics, University of Michigan, Ann Arbor, Michigan

ABSTRACT It is often assumed that upon fusion of the secretory granule membrane with the plasma membrane, lumenal contents are rapidly discharged and dispersed into the extracellular medium. Although this is the case for low-molecular-weight neurotransmitters and some proteins, there are numerous examples of the dispersal of a protein being delayed for many seconds after fusion. We have investigated the role of fusion-pore expansion in determining the contrasting discharge rates of fluorescent-tagged neuropeptide-Y (NPY) (within 200 ms) and tissue plasminogen activator (tPA) (over many seconds) in adrenal chromaffin cells. The endogenous proteins are expressed in separate chromaffin cell subpopulations. Fusion pore expansion was measured by two independent methods, orientation of a fluorescent probe within the plasma membrane using polarized total internal reflection fluorescence microscopy and amperometry of released catecholamine. Together, they probe the continuum of the fusion-pore duration, from milliseconds to many seconds after fusion. Polarized total internal reflection fluorescence microscopy revealed that 71% of the fusion events of tPA-cer-containing granules maintained curvature for >10 s, with approximately half of the structures likely connected to the plasma membrane by a short narrow neck. Such events were not commonly observed upon fusion of NPY-cer-containing granules. Amperometry revealed that the expression of tPA-green fluorescent protein (GFP) prolonged the duration of the prespike foot ~2.5-fold compared to NPY-GFP-expressing cells and nontransfected cells, indicating that expansion of the initial fusion pore in tPA granules was delayed. The $t_{1/2}$ of the main catecholamine spike was also increased, consistent with a prolonged delay of fusion-pore expansion. tPA added extracellularly bound to the lumenal surface of fused granules. We propose that tPA within the granule lumen controls its own discharge. Its intrinsic biochemistry determines not only its extracellular action but also the characteristics of its presentation to the extracellular milieu.

INTRODUCTION

It is often assumed that upon fusion of the secretory granule membrane with the plasma membrane, lumenal contents are rapidly discharged and dispersed into the extracellular medium. Although this is the case for low-molecular-weight neurotransmitters and some proteins, there are numerous examples of the dispersal of a protein being delayed for many seconds after fusion (1–8). A major determinant of the postfusion dynamics is the protein itself and not the cell type. For example, in pancreatic β-cells, fluorescence-tagged C-peptide is discharged within several hundred milliseconds, whereas fluorescence-tagged amyloid polypeptide remains on the cell surface for tens of seconds (4). The discharge of insulin is variable. Insulin is often discharged within several hundred milliseconds, but in ~30% of the fusion events, it remains as a punctum on the cell surface associated with zinc for >30 s (6).

Fluorescence-labeled neuropeptide-Y (NPY) and tissue plasminogen activator (tPA) show contrasting behavior. NPY usually disperses within several hundred milliseconds and tPA after many seconds postfusion in primary chromaffin cells (3), PC12 cells (9) and insulin-secreting cells (5). tPA also disperses many seconds after fusion in an endothelial cell line (10). We confirm the different behaviors of NPY and tPA in this study. Because chromaffin cells express endogenous tPA and NPY in different cell populations, and because the levels of expression of exogenous and endogenous proteins overlap (see our companion article (11)), it is likely that the differing discharge rates for the fluorescence-labeled proteins reflect the discharge rates of the endogenous proteins. In the accompanying article (11), we found that tPA-cerulean (tPA-cer) had a much lower mobility than NPY-cerulean (NPY-cer) within the granule lumen, which in principle could account for its much slower discharge rate after fusion. However, the measured diffusion coefficient (2×10^{-10} cm^2/s) predicts discharge within 1 s if the granule membrane flattens into the plasma membrane within 100 ms after fusion, much faster than the actual time for discharge of ~10 s of fluorescence-tagged tPA.

An alternative explanation for the slow tPA discharge is a long-lived, small-diameter fusion pore that restricts the exit of tPA-cer. Indeed, there is direct evidence that the fusion pore can regulate protein discharge. A dynamin GTPase mutant that slowed fusion-pore expansion caused a detectable slowing of NPY-cer discharge in chromaffin cells (12). Previous studies have also suggested such a sieving property for the fusion pore based upon the different

Submitted November 26, 2013, and accepted for publication April 11, 2014.

*Correspondence: annweiss@umich.edu or holz@umich.edu

Editor: Brian Salzberg.

© 2014 by the Biophysical Society

0006-3495/14/07/0026/8 $2.00

http://dx.doi.org/10.1016/j.bpj.2014.04.064

discharge rates for proteins of different sizes (5,13). However, fusion-pore duration was not measured in these studies, and the possibility that the lumenal protein itself alters fusion-pore expansion was not considered. In this study, we use two techniques to investigate the effects of lumenal protein on fusion-pore expansion. The combination of polarization and total internal reflection fluorescent microscopy (pTIRFM) measured the microscopic distortion of the plasma membrane as an indicator of fusion-pore expansion (14,15). Amperometry probed initial fusion-pore expansion through the measurement of catecholamine release kinetics from individual fusion events in cells expressing tPA-cer or NPY-cer. The results suggest that tPA itself greatly slowed fusion-pore expansion, retarding the rapid discharge of catecholamine and greatly slowing its own discharge.

METHODS

General experimental procedures

Chromaffin cell preparation and transfection were performed as described previously (11). Experiments were performed in a physiological salt solution (PSS) containing 145 mM NaCl, 5.6 mM KCl, 2.2 mM $CaCl_2$, 0.5 mM $MgCl_2$, 5.6 mM glucose, and 15 HEPES, pH 7.4, at ~28°C. Individual cells were perfused through a pipet (100 μm inner diameter) using positive pressure from a computer-controlled perfusion system, DAD-6VM (ALA Scientific Instruments, Westbury, NY). Generally, cells were perfused with PSS for 5 s and then stimulated to secrete with elevated K^+-containing solution (95 mM NaCl, 56 mM KCl, 5 mM $CaCl_2$, 0.5 mM $MgCl_2$, 5.6 mM glucose,15 mM HEPES, pH 7.4) for 60 s.

Immunocytochemistry for confocal imaging

Nonstimulated and elevated K^+-stimulated cells were immediately placed on ice and either incubated immediately with primary antibodies to tPA and dopamine-β-hydroxylase (DBH) (see Fig. 2) or rinsed and incubated with exogenous tPA peptide before adding primary antibodies (see Fig. 5). Cells were then fixed in 4% paraformaldehyde for 30 min, quenched in 50 mM NH_4Cl in phosphate-buffered saline for 30 min, and blocked in 1% gelatin and 4% normal donkey serum before incubation with secondary antibodies.

Antibodies were from goat anti-DBH(Santa Cruz Biotechnology, Santa Cruz, CA); rabbit anti-human tPA (ASMTPA-GF-HT; Molecular Innovations, Novi, MI); AlexaFluor-488, -546, and -647-labeled secondary antibodies (Life Technologies-Molecular Probes, Eugene, OR). Full-length tPA peptide was purchased from Molecular Innovations.

pTIRFM

The specialized excitation system used to create the p-polarization (P-pol) and s-polarization (S-pol) 514 nm beams, superimpose their paths, and further superimpose the 442 nm beam on that path is described in detail elsewhere (12,15). The system is programmed to step through a sequence of three shutter openings (one at a time for each beam), repeating the cycle without additional delay using a TTL triggering system (sequence frequency, 10 Hz). Objective-based TIRF illumination was produced by directing the common beam path through a custom side port to a side-facing filter cube below the objective turret of an Olympus IX70 (inverted) microscope. The filter cube contained the following dichroic mirror/emission filter combination for excitation and emission of cerulean and 1,1′-dioctadecyl-3,3,3′,3′-tetramethylindocarbocyanine perchlorate (DiI): z442/514rpc and z442/514m for NPY-Cer or tPA-Cer/DiI (Chroma Technology, Brattleboro, VT). The beam was focused near the periphery of the back focal plane of a 60× 1.49 NA oil-immersion objective (Olympus, Center Valley, PA) so that the 514 nm laser beam was incident on the coverslip at ~70° from the normal, giving a decay constant for the evanescent field of ~110 nm. Sequential NPY-cer or tPA-cer and DiI S- and P-polarized images (denoted S and P, respectively) were captured using IQ software (Andor, Belfast, United Kingdom). Normalized P-pol emission/S-pol emission (P/S) ratios and P-pol emission + 2(S-pol emission) ($P + 2S$) sums were calculated pixel by pixel for each image, and the transformations were aligned to the NPY-cer images using custom software written in IDL. DiI was added directly to cells bathed in PSS at a 1:50 dilution. The cells were then quickly washed several times in PSS and used immediately. Secretion was stimulated via local perfusion with solution containing elevated K^+ for 60 s, as described above.

Amperometry of individual fusion events

Perfusion solutions and conditions were similar to those used for imaging experiments. Carbon-fiber electrodes encased in glass capillary tubing and sealed with epoxy were manufactured in the laboratory. The electrodes were held at +650 mV and positioned so that they touched the membranes of cells expressing fluorescent protein or nontransfected cells in the same dish. Secretion was stimulated via local perfusion with solution containing elevated K^+ for 60 s. Currents were collected using an Axopatch 200 A amplifier modified for extended voltage output (Axon Instruments, Foster City, CA), filtered at 3 kHz, and sampled at 12 kHz (12,16). No digital filtering was applied. Currents were analyzed using an Igor (Wavemetrics, Portland, OR) (17). Only spikes with amplitudes >10 pA were used in the spike analysis. Prespike foot (PSF) analysis was limited only to those PSFs for which amplitude was >1 pA and duration >2.0 ms.

RESULTS

Characteristics of release of NPY-cer and tPA-cer at individual fusion events

We confirm here numerous aspects of an extensive optical study in chromaffin cells (3), demonstrating differences in release kinetics of labeled, transfected NPY and tPA. We found that NPY-cer dissipates from the fusion site within 100–200 ms of fusion (Fig. 1 *A*) (leaving nothing but background fluorescence). tPA-cer dissipates from sites of release much more slowly, over many seconds (see examples in Fig. 1, *C* and *E*,). tPA-cer fluorescence sometimes increased over several tenths of a second before it began a slow decline (Fig. 1 *E*). Since cerulean fluorescence is insensitive to pH between 5.5 (that of a granule lumen) and 7.4 (that of an extracellular bathing solution) (18) (see also Fig. S1 in the Supporting Material), the increase was not caused by fluorophore response to the pH change upon fusion. It could reflect movement of tPA toward the glass interface after fusion but before discharge into the extracellular space or a change in the fluorophore environment after fusion. If movement is the cause, then the increased intensity would correspond to 19 ± 2 nm ($n = 4$), a small fraction of the granule diameter.

Fusion events were investigated by immunocytochemistry with an anti-tPA antibody. tPA from a transfected cell

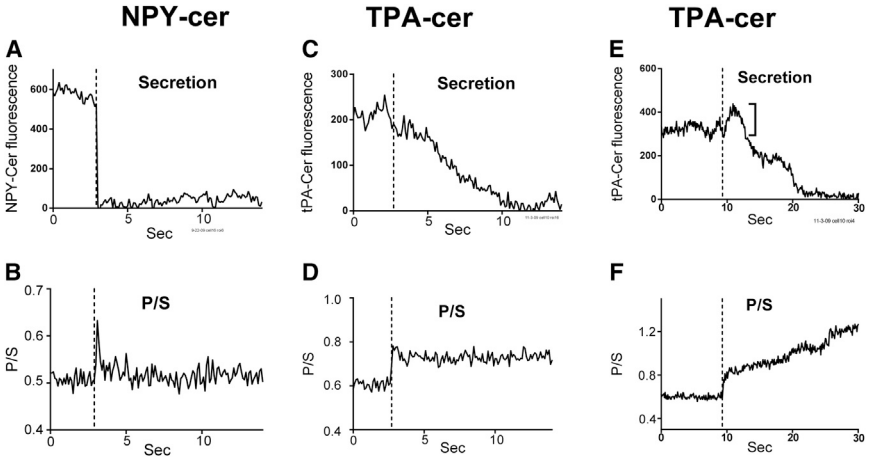

FIGURE 1 NPY-cer and tPA-cer release and fusion pore expansion detected by pTIRFM. (*A* and *B*) Rapid NPY-cer release (*A*) is accompanied by (*B*) a transient change in curvature (*P/S*). (*C–F*) tPA-cer release is slow (*C* and *E*) and is accompanied by long-lived curvature changes (*P/S*) (*D* and *F*). In *E*, cerulean intensity increased (bracket) after the change in curvature, consistent with movement of the granule contents to the glass interface after fusion but before discharge. The abscissa is time after the beginning of perfusion. The vertical dashed lines reflect the estimated time of fusion.

colocalizes with the granule membrane protein DBH on the cell surface for many seconds after fusion (Fig. 2, *A* and *B*), directly demonstrating that released tPA-cer remains punctate at sites of fusion rather than immediately dissipating. Endocytosis is unlikely to significantly reduce the initial exposure of tPA-cer on the cell surface, since virtually no endocytosis occurs within 4 s of depolarization-induced fusion (3,19).

Curvature changes reflecting fusion-pore kinetics of tPA

Curvature at the fusion junction was detected by a combination of polarization and TIRFM (pTIRFM) of an oriented membrane fluorophore, DiI. DiI incorporates into the plasma membrane bilayer with its preferred polarization of light absorption and emission approximately parallel to the local plane of the membrane (20). We described pTIRFM in detail in an earlier publication (15). The technique relies upon the two possible orthogonal electric field polarizations of an evanescent field: one predominantly along the *z* axis (optical axis perpendicular to the coverslip, P-pol) and the other in the plane of the coverslip (S-pol). P-pol excitation will excite membrane DiI with an absorption dipole component that is perpendicular to the coverslip, whereas S-pol will excite only DiI that has an absorption dipole component parallel to the coverslip. The key curvature measurement is an increase in the ratio of the emission with P-pol excitation to the emission with S-pol excitation (*P/S*). We found in this study that the expression of tPA-cer in granules greatly slowed the postfusion flattening of the curved micromorphological structures associated with fusion. Movies S1 and S2 vividly demonstrate the differences in discharge rates and changes in *P/S* and $P + 2S$ (see below) upon fusion of tPA-cer- and NPY-cer-containing granules.

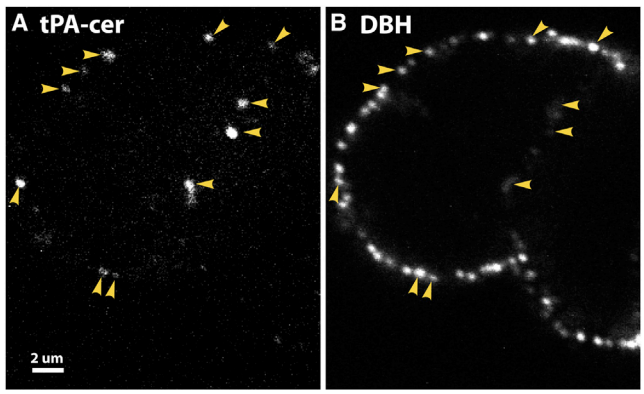

FIGURE 2 Secreted tPA-cer remains at release sites on the plasma membrane after fusion. Chromaffin cells were stimulated with elevated K^+ for 10 s, placed on ice, and incubated with antibodies to tPA (*A*) and DBH (*B*) to mark release sites. Since the cells were not permeabilized, only antigens present on the surface of the cells are visible. Arrowheads indicate colocalization of tPA-cer and DBH. Scale bar, 2 μm. To see this figure in color, go online.

Fig. 1 shows examples of curvature changes associated with fusion of particular granules (a NPY-cer granule (Fig. 1, *A* and *B*) and two different tPA-cer granules (Fig. 1, *C–F*)). The curvature change upon fusion of the NPY-cer granule (Fig. 1 *B*) was transient, lasting for only several tenths of a second. In contrast, the curvature changes upon fusion of the tPA-cer granules (Fig. 1, *D* and *F*) were long-lived, lasting for >10 s. Indeed, the duration of the curvature changes upon fusion of tPA-cer granules was typically much longer than that upon fusion of NPY-cer granules (Fig. 3 *A*). *P/S* durations >10 s occurred in 71% of the fusion events of tPA-cer granules (20/28) and 14% of fusion events of NPY-cer granules (4/28).

We investigated the relationship between the kinetics of tPA-cer or NPY-cer discharge rates after fusion and the duration of stable, fusion-pore-related curvature changes detected by pTIRFM. Discharge rates were measured as the reciprocal of the $t_{1/2}$ of the decline in tPA-cer or NPY-cer fluorescence. For NPY-cer, discharge rates were $\geq$10/s (the time resolution of the measurements) for 27 of 28 fusion events (Fig. 3 *B*). These rapid discharge rates were

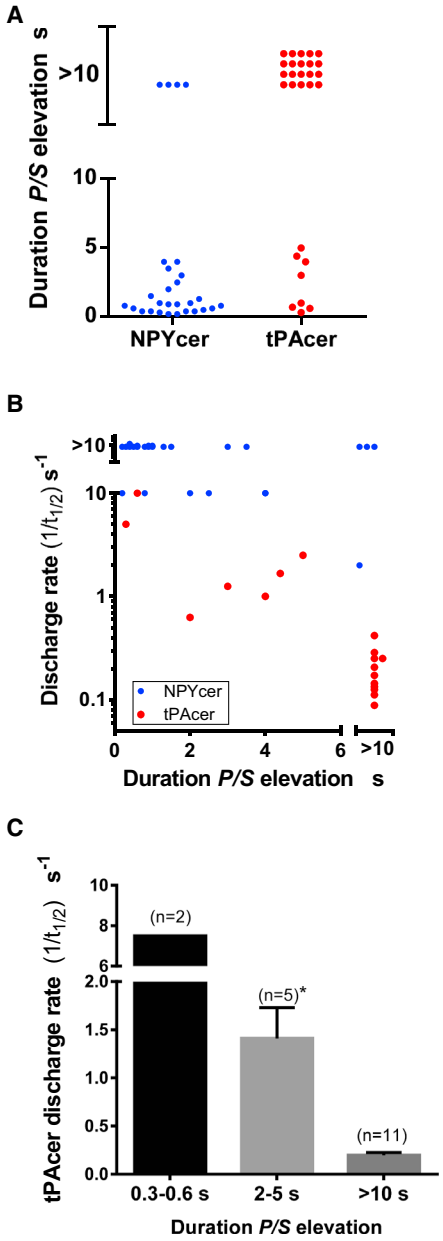

FIGURE 3 Fusion-pore expansion and protein release. (*A*) Distinct fusion pore expansion characteristics (*P/S*) for tPA- and NPY-containing granules. Of these granules, 0.14 of the NYP-cer containing (4/28) and 0.71 of the tPA-cer containing granules (20/28) had stable *P/S* durations of >10 s. (*B*) Relationship of NPY-cer and tPA-cer discharge rates and duration of *P/S* elevations. The discharge rate occurring upon elevation of *P/S* was calculated as the reciprocal of the $t_{1/2}$ of the decline in NPY-cer or tPA-cer fluorescence. Many NPY-cer discharge events were too rapid to resolve (>10/s). (*C*) tPA-granule fusion events from *B* were binned into three groups according to their duration of *P/S* elevation. $^*p < 0.0001$ compared to >10 s *P/S* elevations. There are fewer tPA fusion events in *B* and *C* than in *A*, because discharge rates could not be determined in some of the events due to high background fluorescence in the secretion channel. To see this figure in color, go online.

independent of the duration of *P/S* elevation. In contrast, 17 of 18 fusions of tPA-cer granules had a discharge rate of <10/s and the discharge rates were inversely related to *P/S* duration. This inverse relationship is highlighted in the binned data for tPA (Fig. 3 *C*). The rare elevations of *P/S* that were especially short-lived (0.3–0.6 s, $n = 2$) had discharge rates 40-fold greater than those of long-lived elevations (>10 s, $n = 11$). The *P/S* elevations of intermediate duration (2–5 s, $n = 5$) had discharge rates sevenfold greater than those of long-lived *P/S* changes. Although we cannot measure fusion-pore size directly using pTIRFM, the inverse relationship between tPA discharge rates and curvature duration suggests that the fusion pore detected by pTIRFM limits tPA-cer exit from the fused granule.

The linear combination of the emissions $P + 2S$ approximately reports total DiI emission as observed by a 1.49 NA objective, which in theory is proportional to the amount of DiI at any *xyz* location multiplied by the exponentially decaying evanescent field intensity (15). Computer simulations (15) indicate that $P + 2S$ will increase if the geometry results in more DiI-labeled membrane close to the glass interface, as when a fused granule is attached to the plasma membrane by a short narrow neck. $P + 2S$ will decrease if DiI diffuses into a postfusion membrane indentation, placing DiI farther from the substrate and thereby in a less intense region of the evanescent field. $P + 2S$ is not as robust a measurement as *P/S*, because an increase, decrease, or no detectable change in $P + 2S$ is possible depending upon various countervailing tendencies arising from the geometrical details of the membrane deformation. Nevertheless, 20 fusions of tPA-cer-containing granules (indicated by a sudden change in *P/S*) had measurable changes in $P + 2S$ (16 increased and 4 decreased) and of these, 11 (55%) had increases in $P + 2S$ that lasted >10 s and two (10%) had decreases in $P + 2S$ that lasted >10 s (Table 1). The 11 events with long-lived $P + 2S$ increases correspond to 55% of the long-lived *P/S* increases. In contrast, of the 23 NPY-cer fusions with measurable changes in $P + 2S$, only two (9%) had $P + 2S$ increases lasting >10 s. These data suggest that the presence of tPA-cer in chromaffin granules preferentially stabilizes a geometry that occurs soon after fusion, with the granule membrane connected to the plasma membrane through a short narrow neck. Using a different approach, Almers and colleagues probably detected similar

TABLE 1 Summary of curvature changes lasting >10 s detected by pTIRFM

		$P + 2S > 10$ s	
	P/S > 10 s	Increase	Decrease
NPY-cer	14% (4/28)	9% (2/23)	9% (2/23)
tPA-cer	71% (20/28)	55% (11/20)	10% (2/20)

Fractions in parentheses indicate the number of the changes divided by the total number of measurements. There are smaller numbers of $P + 2S$ changes than *P/S* changes because $P + 2S$ is not as robust a measurement as *P/S*, resulting in some fusion events without significant changes in $P + 2S$ (see text). The 11 events of tPA-cer granules with increases in $P + 2S$ were among the 20 events ($11/20 = 0.55$) with long-lived *P/S*.

structures upon fusion of tPA-Venus-containing granules in PC12 cells (9).

Amperometric detection of catecholamine release from NPY-GFP- and tPA-GFP-expressing cells

Early fusion-pore dynamics can be inferred from amperometric measurement of the kinetics of catecholamine release upon fusion of individual granules. Amperometric current representing the release of catecholamine from individual vesicles (Fig. 4 *A*) was recorded upon stimulation of cells with elevated K^+. Most of the catecholamine release during an individual fusion event is accounted for by the amperometric current spike, which reflects rapid transmitter release through a fusion pore that has partially or completely widened (21–23). The prespike foot (PSF) which is detected in a fraction of the amperometric events, reflects catecholamine released through the initial narrow fusion pore before subsequent expansion (24).

The frequency of amperometric events with PSFs was similar among the groups (tPA-GFP-expressing cells, 41%; NPY-GFP-expressing cells, 45%; nontransfected cells, 37%). However, tPA-GFP-expressing cells had a mean foot duration of 21.5 ± 4.6 ms, significantly longer than that of NPY-GFP-expressing cells (8.23 ± 1.16 ms) and nontransfected cells (9.30 ± 2.25 ms) (Fig. 4 *B*). The analysis represents the average of the medians from individual cells. A cumulative histogram combining all of the individual PSFs indicates that tPA-GFP specifically increased the frequency of a distinct population of long-lived PSFs (Fig. 4 *C*). PSF durations >80 ms occurred with frequencies of 5.3%, 2.7%, and 13% for nontransfected, NPY-GFP-expressing, and tPA-GFP-expressing cells, respectively.

The half-width ($t_{1/2}$) of the catecholamine spike also increased by 50% in tPA-GFP expressing cells compared to NPY-GFP-expressing and nontransfected cells (Fig. 4 *D*). Catecholamine release per event was unaltered by expression of NPY-GFP; it was reduced by 20% by expression of tPA-GFP (Fig. S2).

Exogenous tPA peptide binds to the exposed lumenal surface of fused chromaffin granules

We investigated by immunocytochemistry whether exogenous extracellular tPA peptide binds to the lumenal surface of fused chromaffin granules. The chromaffin granule membrane retains its identity as a distinct domain in the plasma membrane for tens of seconds to minutes after fusion (19,25). Chromaffin cells were incubated at 34°C for 20 s with or without solution containing elevated K^+. Cells

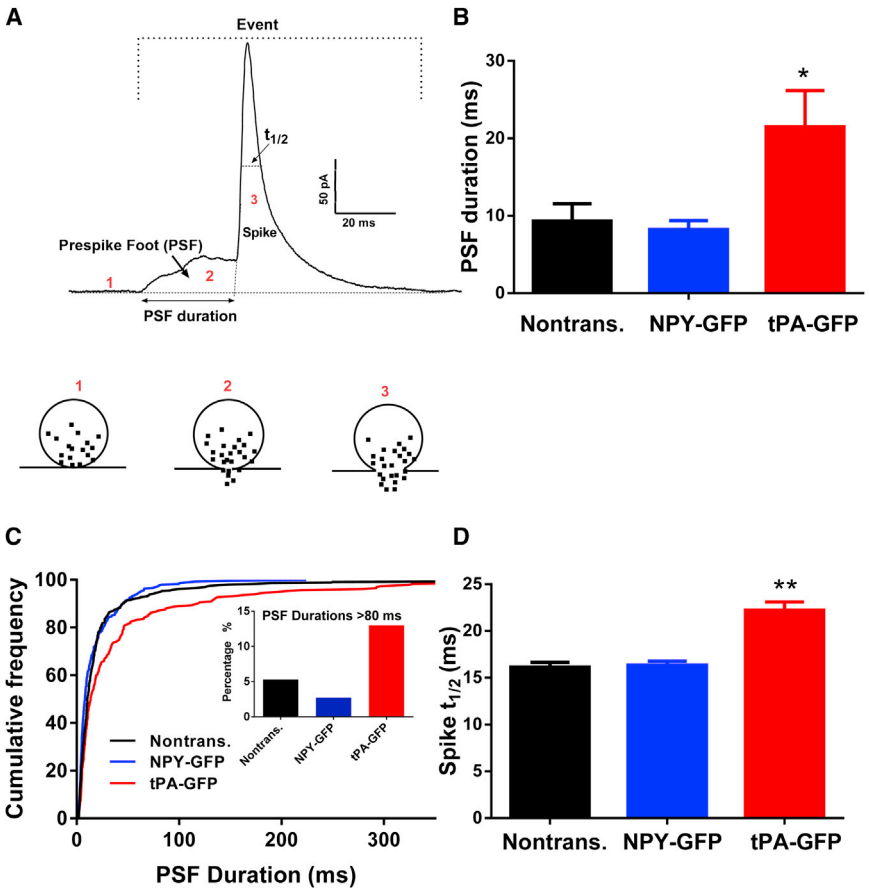

FIGURE 4 Amperometry of tPA-GFP- and NPY-GFP-expressing cells. (*A*) Example of a single amperometric spike illustrating the analyzed parameters. Numbers in figure indicate the granule before (*1*) and at (*2*) fusion pore formation, and upon further expansion of the fusion pore (*3*). (*B*) PSF durations. The average of the median PSF durations in each cell was determined for cells expressing tPA-GFP (14 cells), NPY-GFP (13 cells) and nontransfected cells (15 cells). $*p < 0.003$ compared to either NPY-GFP-expressing cells or nontransfected cells. (*C*) Cumulative frequency distribution of PSF durations for tPA-GFP-expressing cells (248 prespike feet), NPY-GFP-expressing cells (294 PSF) and nontransfected cells (318 PSF). (*D*) Spike half-widths. $**p < 0.0001$ compared to NPY-GFP-expressing cells and non-transfected cells. To see this figure in color, go online.

were rinsed extensively for 15 min at 4°C to remove any secreted tPA that remained associated with the granule membrane at fusion sites. Cells were then incubated with tPA peptide (100 nM) for 30 min at 4°C. Immunocytochemistry revealed that the exogenous tPA bound to the fused granule membrane, which was identified by an endogenous marker of the lumenal surface of the granule, DBH (Fig. 5). tPA binding at this low concentration occurred specifically on the lumenal surface of fused granules.

DISCUSSION

The key finding of this study is that the expression of tPA-cer (but not NPY-cer) within granules greatly slows fusion-pore expansion, an effect that likely contributes to the slow discharge of the protein. Fusion pore expansion was measured by two independent methods, amperometry and pTIRFM, that together probe the continuum from milliseconds (amperometry) to 0.1 s to tens of seconds (pTIRFM) after fusion. The very earliest measure of the fusion pore, the PSF of slowly released catecholamine, was prolonged 2.5 times. The PSF is associated with the initial 2- to 3-nm-diameter fusion pore (24), too narrow to allow protein release. The subsequent amperometric spike was prolonged, consistent with a continuing effect of tPA on the expanding fusion pore. Because some granules in transfected cells do not contain transfected protein, and because the amperometric events were acquired without knowing whether the fusing granules contained tPA-cer, the effects of lumenal tPA on catecholamine discharge are likely to be underestimated.

pTIRFM directly detects membrane curvature changes associated with fusion events by determining the orientation of a membrane fluorophore, DiI (12,15). It demonstrated that after most of the fusion events of tPA-cer-containing granules, curvature was maintained for >10 s, with at least half of the structures having characteristics of a fused granule connected to the plasma membrane by a short narrow neck. Such long-lived events were uncommon upon fusion of NPY-cer-containing granules. It is important to note that the tPA-cer discharge rate was inversely related to the duration of curvature (Fig. 3, *B* and *C*), which is consistent with a stable, narrow fusion pore that restricts protein discharge.

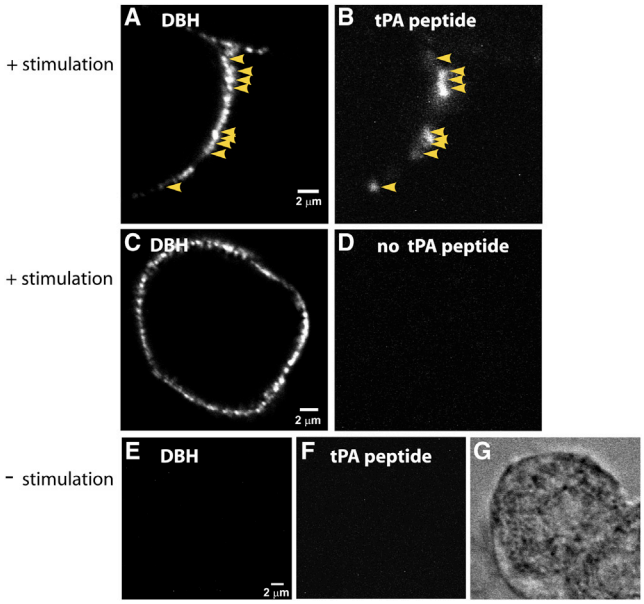

FIGURE 5 tPA peptide binds to DBH puncta on the surface of stimulated chromaffin cells. Chromaffin cells were stimulated for 20 s with 56 mM K^+ at 34°C. The stimulation solution was replaced with ice-cold buffer containing 5.6 mM K^+ and the cells were immediately placed on ice and rinsed for 15 min to remove endogenous tPA from release sites. Cells were then incubated with (*A*, *B*, *E–G*) or without (*C* and *D*) 100 nM tPA peptide for 30 min on ice, followed by extensive rinsing. All cells were then incubated with antibodies to endogenous tPA (*B*, *D*, and *F*) and the lumenal domain of DBH (*A*, *C*, and *E*) for 60 min on ice and then processed and imaged by confocal microscopy. Yellow arrowheads in *A* and *B* indicate instances of colocalization of tPA peptide and DBH. The bright-field image in *G* is the unstimulated cell shown in *E* and *F*. Scale bars, 2 μm. To see this figure in color, go online.

Possible mechanisms for the effect of tPA slowing fusion-pore expansion

tPA peptide added to the extracellular medium bound to the lumenal surface of the granule membrane that was exposed after secretion (Fig. 5). tPA within a granule may also interact with the granule membrane, thereby altering fusion-pore expansion. Direct stabilization of the fusion pore is reminiscent of the effect of a dynamin1 mutant (T65A) with greatly reduced GTPase activity (12). (Dynamin, the master controller of fission in endocytosis, also regulates fusion-pore expansion (5,12,15,26).) The low-GTPase mutant increases the frequency of narrow-necked structures in a way similar to that observed with tPA-cer (12). In contrast to dynamin, the profound effect of tPA-cer on fusion-pore expansion would occur from within the granule lumen, rather than from the cytosol. Protein interactions can strongly alter membrane shape and bending (27–31). Because curvature was sometimes maintained even after the dispersal of detectable tPA-cer, relatively few molecules may be required to stabilize the pore. There is precedent for lumenal interactions influencing fusion-pore expansion: high extracellular Ca^{2+} alters fusion-pore dynamics (32).

Alternatively, the sorting of tPA into a budding granule in the *trans*-Golgi network could influence the lipid or protein composition of the newly formed granule membrane, thereby indirectly altering subsequent fusion-pore dynamics. Differences in membrane components of tPA-containing and non-tPA-containing granules are unknown.

Live-cell imaging provides evidence for extracellular, poorly soluble aggregates after fusion in lactotrophs (2) and pancreatic β-cells (6) (but not in nontransfected chromaffin

cells (2)). There are several reasons why it is unlikely that a postfusion aggregate containing tPA is responsible for the slowing of the initial fusion-pore expansion detected by amperometry or the subsequent stable, narrow-necked structure suggested by pTIRFM. First, curvature was sometimes observed to last after the discharge of virtually all detectable tPA-cer (Fig. 1, *C–F*, and Movie S1, *red and white circles*). Second, although tPA-cer has reduced mobility within the granule, all of it appears to be mobile or participating in a dynamic equilibrium between mobile and immobile forms (11). Finally, tPA has greater solubility at neutral than at acidic pH (33), suggesting that upon fusion its solubility would be increased.

Minimal dimensions of the tPA-stabilized fusion pore

The slow discharge of tPA permits an estimate for the dimension of the stabilized fusion pore. Substantial expansion of the fusion pore would be required for tPA, with a hydrodynamic diameter of 13 × 10 nm (34), to exit from the fused granule. We estimated by simulation in the accompanying article (11) a lower limit for the fusion-pore diameter based upon the average $t_{1/2}$ of tPA-cer discharge after fusion of ~6 s and the mobility of tPA-cer within the granule, 2×10^{-10} cm^2/s. The data are compatible with a granule connected to the extracellular medium through a stable 14- to 15-nm-diameter pore, approximately a nanometer larger than the size of a tPA molecule. However, these considerations probably underestimate the inner pore diameter. The size estimate for tPA does not take into account the covalently attached GFP variant, cerulean. GFP has dimensions of 4.2 × 2.4 nm (35). Furthermore, the simulation assumes a very high mobility through the pore. The movement of tPA-cer through the pore with a diameter only a little larger than its dimensions would likely be significantly retarded because of interaction with the wall. A stable, partially open fusion pore has precedent. Fusion of Weibel-Palade bodies containing von Willebrand's factor in endothelial cells results in stable 12-nm-diameter pores (36).

The sieving properties of a fusion pore responsible for the simultaneous discharge of both NPY and tPA was investigated in granules coexpressing the proteins (tagged with different fluorophores) (3). Upon fusion, tPA was discharged slowly (over seconds), whereas NPY was discharged more rapidly (within 0.5 s). Although experiments have not been performed to investigate fusion-pore dynamics of these events, the results are consistent with a stabilized, narrow fusion pore that more strongly restricts the discharge of tPA-cer than that of the smaller NPY-cer.

Physiological implications

That the intrinsic biochemical characteristics of tPA are important not only for its extracellular proteolytic activity but also for determining its postfusion discharge rate has physiological implications. Evolutionary pressures may have resulted in a secreted molecule that controls its own presentation to the extracellular environment. In addition to the well known role of tPA in fibrinolysis, tPA also has autocrine/paracrine function on adrenal medullary cells (37,38). Secreted tPA activates extracellular plasminogen, which in turn proteolyzes released chromogranin A. A resulting peptide inhibits subsequent secretion through blockade of nicotinic cholinergic receptors. The slow postfusion discharge of tPA at the cell surface likely influences the kinetics of the proteolytic pathway.

Adrenal chromaffin cells normally express tPA and NPY (37,39–41). We found that the proteins are in different subpopulations of primary chromaffin cells in monolayer culture (20% and 4%, respectively) (11). The very different dynamics of the expanding fusion pore for cells expressing different proteins may partially explain the intrinsic variability of responses in a nontransfected population of chromaffin cells.

These results in chromaffin cells probably apply to tPA secretion in other tissues where tPA is expressed (e.g., endothelial cells (42) and posterior pituitary (43) and hippocampal (44) neurons). They may also apply to other proteins, such as brain-derived neurotrophic factor (8,45), that are poorly discharged after fusion.

SUPPORTING MATERIAL

Two figures and two movies are available at http://www.biophysj.org/biophysj/supplemental/S0006-3495(14)00568-2.

We thank Dr. Daniel A. Lawrence, University of Michigan Dept. of Internal Medicine, for the gift of tPA antibody.

This work was supported by National Institutes of Health (NIH) grants R01-NS38129, R56-NS38129, and R21-NS073686 to R.W.H. and D.A., an NIH postdoctoral fellowship, T32-HL-007853, to A.N.W., and NIH postdoctoral fellowships T32-DA007268 and F32-GM086169 and an American Heart Association grant (13SDG14420049) to A.A. This work benefited from a subsidy for DNA sequencing from the University of Michigan Comprehensive Cancer Center.

REFERENCES

1. Kaplan, D. R., J. R. Colca, and M. L. McDaniel. 1983. Insulin as a surface marker on isolated cells from rat pancreatic islets. *J. Cell Biol.* 97:433–437.

2. Angleson, J. K., A. J. Cochilla, …, W. J. Betz. 1999. Regulation of dense core release from neuroendocrine cells revealed by imaging single exocytic events. *Nat. Neurosci.* 2:440–446. http://dx.doi.org/10.1038/8107.

3. Perrais, D., I. C. Kleppe, …, W. Almers. 2004. Recapture after exocytosis causes differential retention of protein in granules of bovine chromaffin cells. *J. Physiol.* 560:413–428.

4. Michael, D. J., X. Geng, …, R. H. Chow. 2004. Fluorescent cargo proteins in pancreatic β-cells: design determines secretion kinetics at exocytosis. *Biophys. J.* 87:L03–L05.

5. Tsuboi, T., H. T. McMahon, and G. A. Rutter. 2004. Mechanisms of dense core vesicle recapture following "kiss and run" ("cavicapture") exocytosis in insulin-secreting cells. *J. Biol. Chem.* 279:47115–47124.
6. Michael, D. J., R. A. Ritzel, …, R. H. Chow. 2006. Pancreatic β-cells secrete insulin in fast- and slow-release forms. *Diabetes.* 55:600–607.
7. Lynch, K. L., R. R. L. Gerona, …, T. F. J. Martin. 2008. Synaptotagmin-1 utilizes membrane bending and SNARE binding to drive fusion pore expansion. *Mol. Biol. Cell.* 19:5093–5103.
8. Xia, X., V. Lessmann, and T. F. Martin. 2009. Imaging of evoked dense-core-vesicle exocytosis in hippocampal neurons reveals long latencies and kiss-and-run fusion events. *J. Cell Sci.* 122:75–82. http://dx.doi.org/10.1242/jcs.034603.
9. Taraska, J. W., D. Perrais, …, W. Almers. 2003. Secretory granules are recaptured largely intact after stimulated exocytosis in cultured endocrine cells. *Proc. Natl. Acad. Sci. USA.* 100:2070–2075.
10. Suzuki, Y., H. Mogami, …, T. Urano. 2009. Unique secretory dynamics of tissue plasminogen activator and its modulation by plasminogen activator inhibitor-1 in vascular endothelial cells. *Blood.* 113:470–478. http://dx.doi.org/10.1182/blood-2008–03–144279.
11. Weiss, A. N., M. A. Bittner, …, R. W. Holz, D. Axelrod. 2014. Protein mobility in secretory granules. *Biophys. J.* 106
12. Anantharam, A., M. A. Bittner, …, D. Axelrod, R. W. Holz. 2011. A new role for the dynamin GTPase in the regulation of fusion pore expansion. *Mol. Biol. Cell.* 22:1907–1918.
13. Barg, S., C. S. Olofsson, …, P. Rorsman. 2002. Delay between fusion pore opening and peptide release from large dense-core vesicles in neuroendocrine cells. *Neuron.* 33:287–299.
14. Sund, S. E., J. A. Swanson, and D. Axelrod. 1999. Cell membrane orientation visualized by polarized total internal reflection fluorescence. *Biophys. J.* 77:2266–2283.
15. Anantharam, A., B. Onoa, …, R. W. Holz, D. Axelrod. 2010. Localized topological changes of the plasma membrane upon exocytosis visualized by polarized TIRFM. *J. Cell Biol.* 188:415–428.
16. Lam, A. D., P. Tryoen-Toth, …, E. L. Stuenkel. 2008. SNARE-catalyzed fusion events are regulated by Syntaxin1A-lipid interactions. *Mol. Biol. Cell.* 19:485–497.
17. Mosharov, E. V., and D. Sulzer. 2005. Analysis of exocytotic events recorded by amperometry. *Nat. Methods.* 2:651–658. http://dx.doi.org/10.1038/nmeth782.
18. Rizzo, M. A., G. H. Springer, …, D. W. Piston. 2004. An improved cyan fluorescent protein variant useful for FRET. *Nat. Biotechnol.* 22:445–449.
19. Bittner, M. A., R. L. Aikman, and R. W. Holz. 2013. A nibbling mechanism for clathrin-mediated retrieval of secretory granule membrane after exocytosis. *J. Biol. Chem.* 288:9177–9188. http://dx.doi.org/10.1074/jbc.M113.450361.
20. Axelrod, D. 1979. Carbocyanine dye orientation in red cell membrane studied by microscopic fluorescence polarization. *Biophys. J.* 26: 557–573.
21. Wightman, R. M., J. A. Jankowski, …, O. H. Viveros. 1991. Temporally resolved catecholamine spikes correspond to single vesicle release from individual chromaffin cells. *Proc. Natl. Acad. Sci. USA.* 88:10754–10758.
22. Chow, R. H., L. von Rüden, and E. Neher. 1992. Delay in vesicle fusion revealed by electrochemical monitoring of single secretory events in adrenal chromaffin cells. *Nature.* 356:60–63.
23. Zhou, Z., S. Misler, and R. H. Chow. 1996. Rapid fluctuations in transmitter release from single vesicles in bovine adrenal chromaffin cells. *Biophys. J.* 70:1543–1552.
24. Albillos, A., G. Dernick, …, M. Lindau. 1997. The exocytotic event in chromaffin cells revealed by patch amperometry. *Nature.* 389:509–512.
25. Ceridono, M., S. Ory, …, S. Gasman. 2011. Selective recapture of secretory granule components after full collapse exocytosis in neuroendocrine chromaffin cells. *Traffic.* 12:72–88.
26. González-Jamett, A. M., X. Báez-Matus, …, A. M. Cárdenas. 2010. The association of dynamin with synaptophysin regulates quantal size and duration of exocytotic events in chromaffin cells. *J. Neurosci.* 30:10683–10691.
27. Elgsaeter, A., B. T. Stokke, …, D. Branton. 1986. The molecular basis of erythrocyte shape. *Science.* 234:1217–1223.
28. Markin, V. S., and M. M. Kozlov. 1988. Mechanical properties of the red cell membrane skeleton: analysis of axisymmetric deformations. *J. Theor. Biol.* 133:147–167.
29. Raucher, D., T. Stauffer, …, T. Meyer. 2000. Phosphatidylinositol 4,5-bisphosphate functions as a second messenger that regulates cytoskeleton-plasma membrane adhesion. *Cell.* 100:221–228.
30. McMahon, H. T., M. M. Kozlov, and S. Martens. 2010. Membrane curvature in synaptic vesicle fusion and beyond. *Cell.* 140:601–605.
31. Wang, S., E. Martin, …, M. Glaser. 1988. Distribution of phospholipids around gramicidin and D-β-hydroxybutyrate dehydrogenase as measured by resonance energy transfer. *Biochemistry.* 27:2033–2039.
32. Alés, E., L. Tabares, …, G. Alvarez de Toledo. 1999. High calcium concentrations shift the mode of exocytosis to the kiss-and-run mechanism. *Nat. Cell Biol.* 1:40–44.
33. Nguyen, T. H., and C. Ward. 1993. Stability characterization and formulation development of alteplase, a recombinant tissue plasminogen activator. *Pharm. Biotechnol.* 5:91–134.
34. Margossian, S. S., H. S. Slayter, …, J. McDonagh. 1993. Physical characterization of recombinant tissue plasminogen activator. *Biochim. Biophys. Acta.* 1163:250–256.
35. Ormö, M., A. B. Cubitt, …, S. J. Remington. 1996. Crystal structure of the *Aequorea victoria* green fluorescent protein. *Science.* 273:1392–1395.
36. Babich, V., A. Meli, …, T. Carter. 2008. Selective release of molecules from Weibel-Palade bodies during a lingering kiss. *Blood.* 111:5282–5290.
37. Parmer, R. J., M. Mahata, …, L. A. Miles. 1997. Tissue plasminogen activator (t-PA) is targeted to the regulated secretory pathway. Catecholamine storage vesicles as a reservoir for the rapid release of t-PA. *J. Biol. Chem.* 272:1976–1982.
38. Parmer, R. J., M. Mahata, …, L. A. Miles. 2000. Processing of chromogranin A by plasmin provides a novel mechanism for regulating catecholamine secretion. *J. Clin. Invest.* 106:907–915.
39. Kristensen, P., D. M. Hougaard, …, K. Danø. 1986. Tissue-type plasminogen activator in rat adrenal medulla. *Histochemistry.* 85:431–436.
40. Steiner, H. J., K. W. Schmid, …, H. Winkler. 1989. Co-localization of chromogranin A and B, secretogranin II and neuropeptide Y in chromaffin granules of rat adrenal medulla studied by electron microscopic immunocytochemistry. *Histochemistry.* 91:473–477.
41. Kuramoto, H., H. Kondo, and T. Fujita. 1986. Neuropeptide tyrosine (NPY)-like immunoreactivity in adrenal chromaffin cells and intraadrenal nerve fibers of rats. *Anat. Rec.* 214:321–328. http://dx.doi.org/10.1002/ar.1092140312.
42. Loscalzo, J., and E. Braunwald. 1988. Tissue plasminogen activator. *N. Engl. J. Med.* 319:925–931. http://dx.doi.org/10.1056/NEJM198810063191407.
43. Miyata, S., Y. Nakatani, …, T. Nakashima. 2005. Matrix-degrading enzymes tissue plasminogen activator and matrix metalloprotease-3 in the hypothalamo-neurohypophysial system. *Brain Res.* 1058:1–9. http://dx.doi.org/10.1016/j.brainres.2005.07.027.
44. Salles, F. J., and S. Strickland. 2002. Localization and regulation of the tissue plasminogen activator-plasmin system in the hippocampus. *J. Neurosci.* 22:2125–2134.
45. Kolarow, R., T. Brigadski, and V. Lessmann. 2007. Postsynaptic secretion of BDNF and NT-3 from hippocampal neurons depends on calcium calmodulin kinase II signaling and proceeds via delayed fusion pore opening. *J. Neurosci.* 27:10350–10364. http://dx.doi.org/10.1523/JNEUROSCI.0692–07.2007.